PROCEEDINGS OF SPIE

SPIEDigitalLibrary.org/conference-proceedings-of-spie

Design and performance characterization of simultaneous reflectance and surface-mapping laser scanner for application in

Frank M. Caimi
Donna M. Kocak
Coy Colquitt

SPIE.

Design and Performance Characterization of Simultaneous Reflectance and Surface Mapping Laser Scanner for Application in Underwater Inspection

Frank M. Caimi*, Donna M. Kocak, Coy Colquitt

Department of Electrical Engineering
Harbor Branch Oceanographic Institution, Inc.
5600 US 1 North
Ft. Pierce, Florida 34946

* Current affiliation Department of Electrical Engineering, Florida Institute of Technology, 150 W. University Blvd., Melbourne, FL 32901, caimi@ee.fit.edu

ABSTRACT

Considerable advancements have been made in undersea imaging over the past decade enabling long-range detection and observation of underwater objects in clear and turbid (cloudy) water. The image transfer characteristics of the medium (i.e. scattering and absorption) have been primary obstacles in developing high performance systems. However, the application of lasers to the imaging formation process is currently providing a means for acquiring long-range images, over 5-6 attenuation lengths in comparison to 1-2 attenuation lengths for more conventional methods. In addition, laser technology is now offering the promise of systems capable of forming range maps and depth resolved images. Range resolution is possible by a variety of methods, such as triangulation, time gating/LIDAR, the formation of Moiré fringes by structured illumination, intensity gradient processing common to shape-from-shading computer vision techniques, and phase sensitive coherent processing using modulated sources. Performance is determined by the optical power available, the system geometry, the detection means, and (primarily by) the optical attenuation of the medium. In spite of the limitations imposed by these effects, a number of range sensitive imaging systems are being developed using various technological approaches, which include: 1) range gated triangulation using an optically coupled image intensifier and lateral effect photodiode, 2) streak camera processing of time histories across multiple returns from line format illumination, 3) triangulation via intensified CCD using narrow, synchronized illumination and detection FOVs, 4) laser coherent modulation with phase sensitive detector array, 5) range-gated ICCD image arrays and, 6) pre- and post-processing image gradient methods using natural illumination.

In this paper we describe the first approach listed above and present results from a recently developed system that produces video-rate, three-dimensional maps of the image space using a scanning laser configuration and a patented micro-channel plate intensified detector. The scene is viewed from a separate location to provide depth information via triangulation. The detector provides an estimate of position of the apparent landing spot of the laser beam for each scan angle from which a depth estimate is calculated. The system is designed to scan an approximate 15 X 15 degree field-of-view at distances from 1.5 to 2.5 meters with a resolution of 1.5 cm at rates of 10-30 full images per second, and can accommodate range gating to reduce scattered light interference.

1. INTRODUCTION

Structured illumination[1], moiré[2], as well as acoustic approaches using high frequency sonar[3] have been successfully implemented for undersea point ranging and contour description. Principles associated with contrast enhancement and long range image formation in strongly scattering media have been developed and applied [4, 12, 16, 17], as well as optical schemes using lasers for the acquisition of dimensional data such as surface maps and contours [2, 11, 15, 16]. Surface mapping schemes based upon machine vision approaches developed in the late seventies are also potentially of interest for some applications. Surface mapping applications include the measurement of geological features; the determination of biological specimen size, shape, or volume; the estimation of movement or behavior characteristics of specific objects; and short-range navigation and station keeping control for robotic vehicles and platforms.

Additional applications include the inspection of undersea structures such as drilling platforms, military systems, ship hulls, cables, pipes, etc., repair tasks or activities that require the positioning of manipulators or tool pieces, biological and geological monitoring activities associated with scientific research and environmental impact studies, as well as military surveillance,

Part of the SPIE Conference on Optical Scanning: Design and Application
Denver, Colorado • July 1999 SPIE Vol. 3787 • 0277-786X/99/$10.00

identification, and detection. Although conventional cameras, including disparity stereo imaging systems, can provide a means for visualization of the work environment, their use is limited in low visibility environments and they do not provide adequate capability for real-time quantitative measurements. Consequently, methods are being investigated by which three-dimensional images or range maps can be formed in difficult environments where scattering and absorption processes are dominant.

2. UNDERWATER IMAGING LIMITATIONS

The acquisition and formation of images in the underwater environment is governed primarily by scattering and absorption processes associated with water and suspended particles. Optical scattering by hydrosols is reasonably well characterized in the literature[4]. In seawater, the scattering dominates in the forward direction, causing a reduction of the MTF at high spatial frequencies, but confining flux primarily in the original launch direction. The amount of scattered light present is determined by the volume scattering function[5, 6], and can be characterized by the volume scattering coefficient s and the volume absorption coefficient a. The assumed relationship of these quantities to the total attenuation coefficient is:

$$\underset{measurable}{c} = \underset{absorp.\,coef.}{a} + \underset{scatter.\,cof.}{s} \tag{1}$$

The "beam attenuation" coefficient c is the sum of both quantities (assuming Raman and fluorescent contributions are negligible) and is typically defined as the reciprocal distance over which the flux in a collimated beam is observed to fall to 1/e of its initial value as measured with a detector having an infinitesimally small angular acceptance angle. Often, the performance of an imaging system is characterized in terms of the reciprocal beam attenuation coefficient in units of meters or as a number n of reciprocal beam attenuation coefficients, i.e. "n-c^{-1}" or "n-alpha^{-1}". Light that is not absorbed or scattered continues in the original direction of propagation and is diminished in strength by a nearly exponential dependence upon distance. The light flux and its direction after reflection from the surface of an object is subject to the same processes as it travels back toward the detector. The number of photons returning from the object in comparison to the number being returned via the scattering process, may be greatly diminished, depending upon the distance, the scattering to absorption cross-section over the angular regions of interest, and the reflectivity of the object. Contrast in the image is reduced by backscattered light arriving at the detector from the entire illuminated volume. The detected signal, if integrated over a sufficiently long time period, can contain little information from *single* reflective image points in the scene, and consequently is usually observed as a background illuminance level that adds non-coherently to the light field originating on, or reflected from, objects in the scene. Light coming from each illuminated point on the object is subject to being spread in such a way that it appears to the observer as though it were coming from a "blur" of points on the object and can be described by a characteristic point spread function.

The relative degree of absorption, in comparison to scattering, depends upon the composition of the suspended matter and upon the types and quantity of dissolved substances and is adequately described elsewhere[5]. The deep ocean optimally passes light in the blue-green portion of the spectrum where attenuation lengths (c^{-1}) of 20 meters are common, while in coastal regions values of 3-5 meters are characteristic with maximums shifted toward the yellow.

If the photon loss due to absorption were the only effect, cameras having low light sensitivity would produce excellent images, requiring only the ability to respond to the unscattered light field returning from the scene. Unfortunately, the scattering coefficient is of the same order of magnitude as the absorption coefficient, causing detail to be lost. Direct scattered photons arrive back into the camera at a time of arrival prior to that of the reflected, unscattered photons, thereby reducing the image contrast. The relative degree of scatter in the forward or backward directions is described by the asymmetry factor g defined by:

$$g = \int_0^{2\pi}\int_0^{\pi} \cos\theta [P(\theta)/4\pi] d\Omega, \tag{2}$$

where $P(\theta)$ is the scalar phase function and θ is the angle with respect to the direction of propagation. The scalar phase function is related to the volume scattering coefficient b and volume scattering function β by:

$$P(\theta) = 4\pi\beta(\theta)/b \tag{3}$$

with b being defined as,

$$b = 2\pi \int_0^{2\pi} \beta(\theta)\sin(\theta)d\theta. \tag{4}$$

The asymmetry factor is zero for isotropic scattering, near minus one for highly backscattering media, and near one for highly forward scattering media. The relative value of *b in* relation to *a* is spectrally variant and for pure water is maximum near the absorption minimum at approximately 475 nm giving water its deep blue color. The volume scattering function is naturally of importance in determining the apparent contrast of in-water images. Its form is approximately characterized for pure water over a limited angular range[7] and is very nearly that expected for Rayleigh scattering:

$$\beta_{water}(\theta) = \beta(\theta)_{90}\left[\frac{\lambda_0}{\lambda}\right]^{4.32}\left[1 + 0.835\cos^2(\theta)\right]. \tag{5}$$

In seawater, the function is considerably forward peaked, but still a minimum at 90 degrees. At near forward angles (milliradians or less) the scattering is described by refractive index variations existing in the medium (turbulence) and may be expressed as an rms variation in refractive index from which is estimated an expected modulation transfer function[8, 9].

Image contrast is governed by the relative magnitudes between the scattering function integrated over the solid angle of view in relation to the exponentially decaying direct image component that is not scattered. The result is highly dependent upon the illumination geometry, the spectral characteristics of the lighting, the ambient illumination, and in the case of artificially illuminated scenes, by the overlap regions between the illumination source and the camera field-of-view. It is generally assumed that images can be formed over one or two attenuation lengths before the image contrast becomes a limiting factor. For illustrative purposes, assume that light is emanating from a point on the surface of an object. At the camera, the illumination field will consist of the sum of two components E_S and E_d, the scattered and direct fields, respectively. These components can be approximated by:

$$E_d = e^{-cz} I / z^2$$

$$E_s = \left(2.5 - 1.5\log_{10}\frac{2\pi}{\varphi}\right)\left[1 + 7\left(\frac{2\pi}{\varphi}\right)^{1/2} e^{-sz}\right]\frac{Ise^{-sz}}{4\pi z} \tag{6}$$

The latter function is empirically derived[6] for a point source and can be evaluated as a function of cz, the attenuation length, and ϕ, the full angle width of the source. As the source becomes narrow in angular extent, the scattered component is reduced, but not nearly as rapidly as the direct component with increasing range. The ratio of direct to scattered illumination is plotted in Figure 1. For a typical *c/s* ratio of 3, the two functions are equal at an attenuation length of about 1 for source angles of π. In reality, more than one point is illuminated and scatter from all other points is summed at the camera, making the situation worse than is described by (6) and Fig. 1. Note that this simple analysis indicates poor contrast at $cz > 2$, or greater than two attenuation lengths as stated.

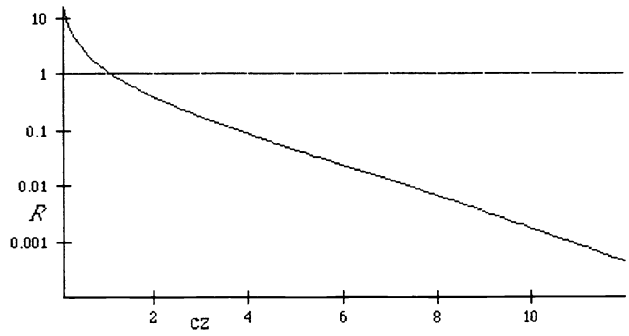

Fig. 1. The ratio R of E_d to E_S versus attenuation length cz for c/s =3.

The primary limitation of the conventional imaging system is the loss of contrast, as shown, but loss of optical flux is also of concern. If the scattered field were not present, the loss would be governed by only the exponential factor in (6). At seven attenuation lengths, the light intensity is reduced to 10^{-5} of its value at one attenuation length. Therefore, low light level cameras such as SIT, ISIT, ICCD, and I^2CCD are commonly used in undersea imaging applications. Since contrast is reduced dramatically by scattering, the signal-to-noise (S/N) ratio of the camera must be sufficient to observe the reflected image light component against the non-coherent scattered light field or "veiling luminance". For this reason, ICCD cameras having exceptional luminance sensitivity but poor S/N may prove to be unacceptable in comparison to SIT types under some circumstances. Although the geometric form of the illuminating beam has not been expressly treated in the discussion above, it should be obvious that narrowing its angular width and reducing the field-of-view of the detector can improve the system performance substantially. There is recent application of this technique to 3-D image formation using triangulation methods[26]. It is also possible to use indirect illumination to reduce the near field backscatter by redirecting the illumination beam to allow geometric overlap at the expected maximum range[10, 25]. In this case, scattered light is responsible for illuminating the object, rather than the direct beam. In this way, the common overlapping volume between the camera and source is minimized and contrast is enhanced. Any system developed for production of range maps must necessarily take into account the scattered light field components as well as the S/N ratio available at the detector.

The physical description of light propagation for imaging purposes has been described Navy sponsored studies[11-13] and can be considered an extension of the single communication channel properties described by others[14]. This research has resulted in the advancement of laser illumination techniques to reduce the backscatter and therefore increase image quality and range via: 1) temporal methods using pulsed illumination and gating to block scattered photons arriving at the camera prior to the arrival of object returned photons, and 2) field limited detection optics in association with synchronous scanning of the object or scene with a small cross-section laser beam. System configurations have also been devised to respond to temporally encoded illumination, thereby reducing interference from background illumination or scatter[28]. Presently, these techniques are being combined with ranging and other methods for producing additional information from a scene, and a variety of systems are being field-tested. Although systems are being developed using phase coherent and time of flight ranging techniques, this paper deals primarily with triangulation schemes for range imaging, as several systems have been constructed and field tested.

3. RANGE IMAGING BY TRIANGULATION

3.1 *Structured Illumination and Scanned Illumination Methods*

Several undersea inspection systems have been developed using laser, structured illumination for producing 3-dimensional data[21]. These systems operate in either a fly-by or slow scan mode and rely upon spatial disparity of the laser projector and sensor to determine range by triangulation. "Fly-by" systems typically use a single laser stripe projection to scan broadside to the direction of motion in order to produce a series of one-dimensional range maps, which are later assembled into a windowed two-dimensional format. By contrast, "scan mode" systems employ a high resolution 2-D laser scanner in addition to a high resolution position sensitive detector, such as a 1-D CCD array to detect the laser reflection at every point of the scan. A two-dimensional range map is produced, but systems developed in the early 1990s operated at a slow rate sometimes taking minutes to form a complete scan image. Advancements in commercial linear and two dimensional imaging arrays now make possible rapid scanning, and at least one system is in development. Techniques for reduction of scattered light interference in these systems rely upon synchronous scanning, range gating, or spatial averaging.

3.2 *Triangulation Based Surface Mapping System*

A short operational range, surface mapping system was developed at Harbor Branch Oceanographic Institution under contract to the Naval Civil Engineering Laboratory[22]. The triangulation based system produced 3-D maps of unhidden surfaces within a 40^{o} field-of-view at a 1-2 meters standoff distance in less than 5 seconds per scan. The apparent position of the laser reflection against the scene was determined with an accuracy of better than 1 part in 1000, providing similar resolution to distinguish differences in range to each point in the scan. Each scan produced a two-dimensional matrix of range values that provided a three-dimensional relief map of the area of interest. The operator was able to view a relief map that could be rotated and viewed from different angles and distances. The extent, positioning, speed, and resolution of the laser scan anywhere within the field-of-view was also under operator control.

The system was configured to raster scan a region of space using a frequency doubled 150 milliwatt Nd:YAG laser with a lateral resolution of 0.05 degrees (approximately 200x200 pixels), or greater (800 x 800 pixels) along both the x and y scan axes. A

two-axis galvo scanner was used. Return light from the laser scanner was observed at an adjacent location. The received light was focused onto a lateral effect photodiode that produced an estimate of the reflected beam location, from which the range coordinate of the surface was computed by triangulation. A diagram of the system geometry is shown in Fig. 2.

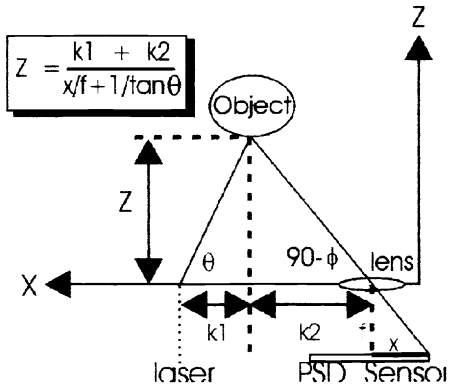

Fig. 2. Configuration of a flying spot laser scanner system used for underwater surface mapping.

Calibration for angular errors due to the scanner and optics was included in the software. In operation, the system was able to map surface features at approximately Z= 0.5-2 meters, with a positional accuracy of 1 millimeter. Design goals were for operation at optical beam attenuation from 0.05- 0.5 m^{-1}. Under these conditions, the system performance was primarily limited by the laser power, the detector aperture size, and by the detector signal-to-noise ratio, limiting the useful range and scan rate to approximately 2 m and 10 kHz/voxel, respectively. The system was able to produce exceptional quality images in air. However, in turbid water (c=0.5m^{-1}), tests indicated inherent distortion arising from scattered light entering the detector aperture, resulting from a skewing of the response function of the position sensitive detector away from the reflected light centroid[23].

3.3 *Triangulation Theory*

Using the system geometry shown in Fig. 2, the laser is scanned through angles θ_X and θ_Y and the separation of the laser scan center and detector axis is BL. The detector produces a measure of the reflected light position along the *x*-axis in the image plane. The *z*-axis position can be estimated from:

$$Z(t) = \frac{BL}{\frac{x(t)}{f} + \frac{1}{\tan\theta(t)}}, \qquad X(t) = Z(t)\frac{x(t)}{f} = Z(t)\tan\varphi \tag{7}$$

where f is the equivalent focal length of an ideal lens forming an image at the detector, BL is the baseline length, and θ_x is the horizontal projection angle, which are known (estimated) quantities. Capital and lower case symbols are referred to the object and image plane coordinate systems, respectively. In order to determine the magnitude of the *z*-coordinate, accurate estimates for *x* and θ_x should be obtained. Although $\theta(t)$ may be derived from the scanner control signals, estimates of $x(t)$ are subject to errors from noise from the detector and scan geometry, as well as from non-ideal behavior of the imaging lens system and variations of the scan center position during the scan as a result of Fresnel refraction at the window interfaces. The noise is due to Johnson and shot effects from the detector, as well as from the preamplifier. Additional sources of noise arise from the intensifier and its power supply. Steps have been taken to reduce these noise contributions. An example of noise arising from a "flat wall" scan is illustrated by the histogram of Fig. 3. This data was taken from initial tests of a system designed for 1:200 z-axis resolution. The deviations from ideal behavior of the lens and window assembly are negated at a particular range via a computer calibration technique that assigns predicted values of θ_x for each point in the scan. This first order correction has proven adequate for scans at sufficiently large object distances.

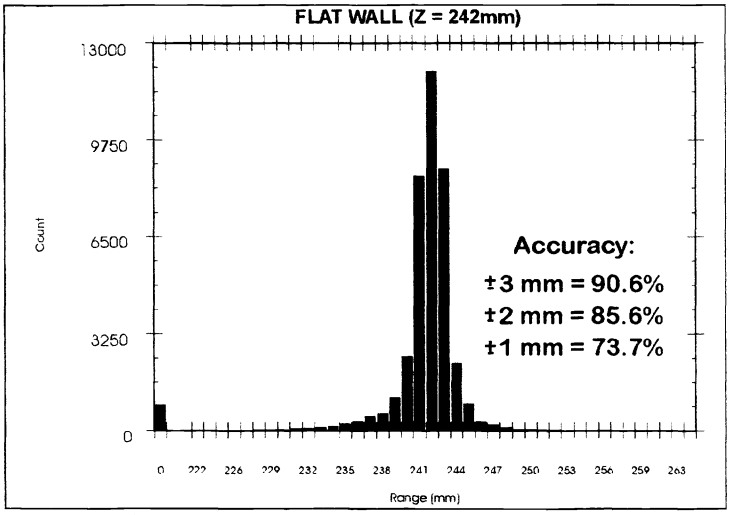

Fig. 3. Range histogram for a flat wall as measured by surface mapping system with 1:200 range resolution.

The z-axis resolution is determined by the x-axis resolution, dx:

$$\frac{dx}{dz} = Kf / z^2 \tag{8}$$

Thus, the resolution is reduced in proportion to the square of the range for a given system geometry and lens focal length. As the range is increased, however, the focal length may also be increased to reduce the FOV. If f is increased in proportion to the range, the percentage change in range (dz/z) will produce the same dx at the detector. Increases in the laser power or detector sensitivity would allow this method to be used at greater standoff distances.

3.4 *Position Estimation Method*

It can be shown that the error in the coordinate geometry originates from side and backscatter from the projected beam, as well as from the scene illumination profile. The amount of scatter can be estimated from a radiometric model that is then used to develop an error function from which a revised and more accurate estimate is made. The detector provides a first estimate of the scene geometry from the computation of the Z coordinate from the x and y position estimates. This information is used to provide a basis for determining an error function, determined from a model from which an improved estimate of the centroid offset can be obtained for each coordinate triad in the image. Alterations in the Z-coordinate estimate can be made at each iteration to offset a reduction in the error function.

Therefore, to correct these turbidity effects, and to obtain a more accurate estimate for the light centroid, an iterative adaptive signal processing estimation technique has been developed[24]. The adaptation algorithm is designed to minimize an appropriate cost function formed by the resulting error due to the distorted measurements in the presence of the turbid conditions. Repeated scans are made in an iterative fashion to reach a desired minimum of the error function. This process improves the accuracy of the positional estimate in a fashion that is independent of the surface location, reflectivity, and size. A greater amount of time is required in the construction of the corrected image (data set) according to the number of iterations required for the desired error reduction. Algorithms for the estimation of the more accurate position of the light centroid may be implemented by a dedicated special purpose digital signal processor, based on data collected.

3.5 *Low power system implementation*

Enhanced performance of the laser mapping system shown in Fig. 2 can be obtained through modification of the original design concept to include image amplification as shown in Fig. 4. Several versions of this system have been developed for different applications requiring standoff distances of 0.2 m and 1.5m, respectively.

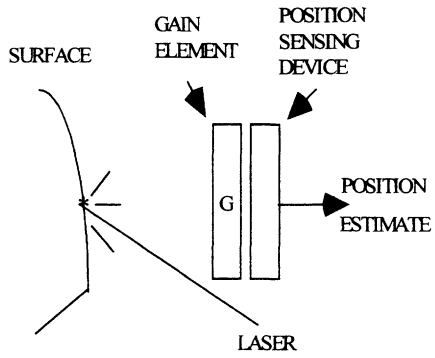

Fig. 4. Advanced Triangulation Concept

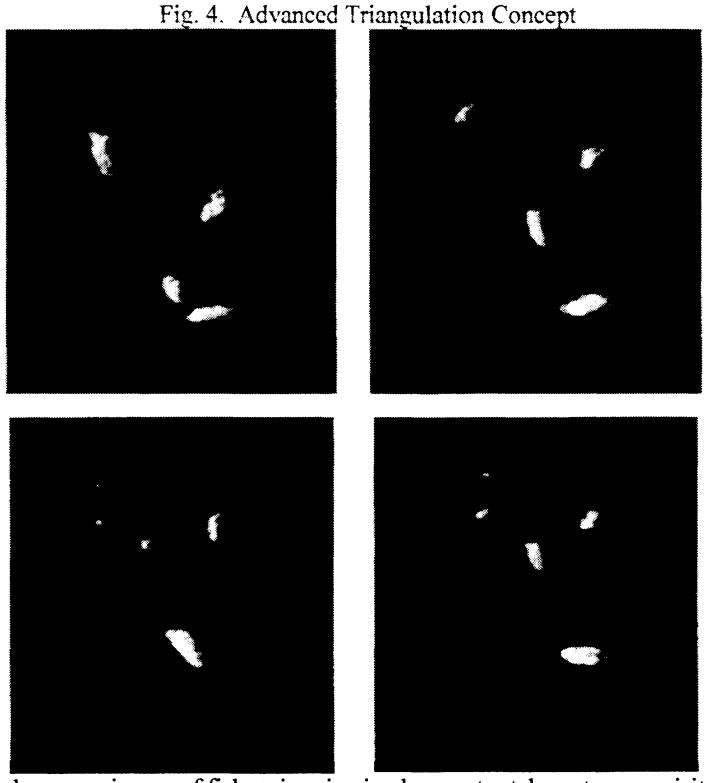

Fig. 5. 3-D pseudo-color range image of fish swimming in clear water taken at an acquisition rate of 20/second.

The gain element G provides the ability to: increase the range Z; to accommodate lower object reflectivity R; and to increase the scan rate because of the nature of the detection process. Typically, a microchannel plate intensifier is used to achieve electron multiplication from a gallium arsenide photocathode. The assembly is coupled to a fast response phosphor, which then is coupled by fused fiber optic taper to a lateral effect photodiode, from which position information is derived. Achievable gains using this methodology have provided a 20 Hz image acquisition rate at range distances of 1 meter using a 10-milliwatt 670 nm scanned laser. An image sequence of fish swimming at 1-meter range is shown in Figure 5. The x, y, and z-axis resolution of the system is 1 part in 200, and the fish are several centimeters in length. Since the scan angle is +/- 15 degrees, the lateral extent of the FOV is about 0.5 meters, implying a lateral resolution of about 3 millimeters and accounting for low resolution. The images produced use pseudo-color encoding for z-axis distance, however, this is not observable in the gray scale images reproduced here. In addition, the tails of the fish are transparent and do not produce a measurable return. Each image was taken from a sequence digitized at a rate of 20 images per second at times of 0.35, 1.15, 1.75 and 2.75 seconds. Post processing of the fish motion was possible using recorded data files. Tracks for the X-Y and X-Z planes over the time sequence are shown in Fig.6.

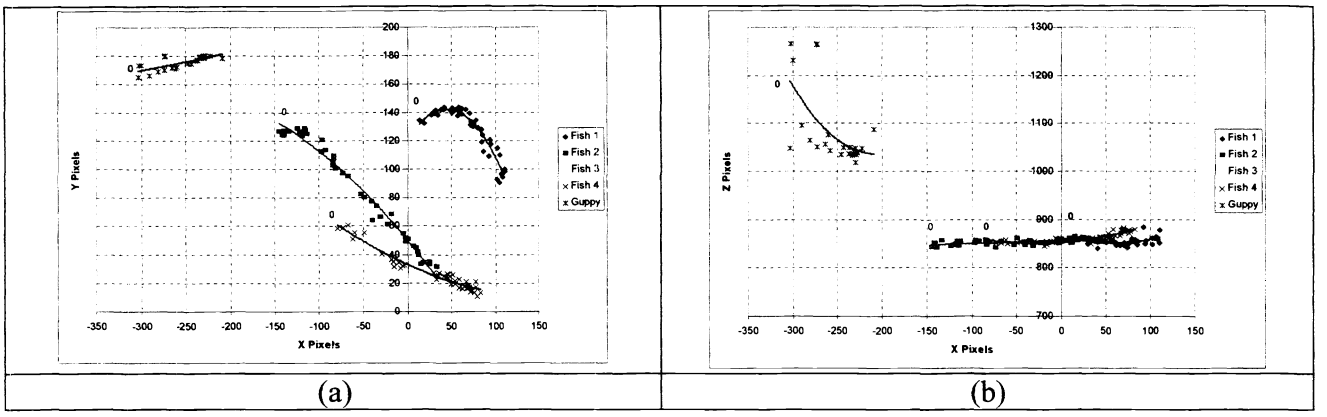

Fig. 6. Motion paths of fish in (a) X-Y plane and (b) X-Z plane.

The gain available from the MCP detection scheme indicated in Fig. 4 provides the ability to reduce the laser power and thereby achieve portable operation, at least at close range. The approximate power arriving at the detector is given by:

$$P_D = \frac{F_{\text{det}} f^2}{8 f_{\#}^2 n_w^2} \tag{9}$$

where f and $f_{\#}$ are the focal length and f-number of the imaging lens, F_{det} is the power leaving the object surface, and n_W is the refractive index of water. A sample calculation using a laser power of 10 mW and typical attenuation factors for 670 nm wavelength, provides an input light level to the gain element of approximately 1 nanowatt at a range of 1 meter distance. The required power at the position sensing device is dependent upon the background noise level at the frequency of operation. A requirement for a 20 Hz scan rate and a 200 x 200 scan resolution predicates an 800 kHz response bandwidth at the detector. Since the inherent noise level is determined by shot and thermal processes (approximately 5 nW noise equivalent power), the required gain must be sufficient to overcome the noise by a sufficient margin to achieve an adequate signal-to-noise ratio. The computation of the range from Eq. 7 at a resolution commensurate with the required range resolution (1 part in 200) necessitates a gain of 1000. The images shown in Fig. 5 were scanned with a system designed using these parameters. It is noteworthy that synchronous scan and range gating techniques are applicable to this system for reduction of scattered light interference. At greater standoff distances and at large inherent attenuation (>0.5 m^{-1}), gating of the MCP is required. Additional advantages of this system are the potential for operation at detector wavelengths different from the scanning source. Ranging systems configured in this way should be useful in terrestrial and underwater detection and localization of fluorescent objects or plumes and may be helpful in the tracking and assessment of weapons of mass destruction.

3.6 Ambient Light Interference Design Considerations

In addition to the previously mentioned effects, light induced interference can be a dominant source of error in any low power system. There are several possibilities to reduce interference from background light: 1) use the attenuation properties of water to screen ambient light by selecting a wavelength of operation that provides the desired degree of attenuation while maintaining sufficient laser signal at the detector; 2) incorporate narrowband filters at the detector aperture to pass only the laser linewidth; 3) temporally modulate the laser and synchronously detect the return; 4) reduce the angular aperture of the detector and synchronously scan, if necessary; 5) operate in deep water or at night.

Selection of laser wavelength is a particularly attractive method whereby the surrounding medium acts as an effective optical filter. Requirements for effective use of this option are to ensure that the distance from the source of interference to the detector aperture is much greater than the distance to the object. For short-range applications less than several meters, this condition is usually fulfilled. The wavelength is chosen to provide an acceptable attenuation factor from the laser to the subject, while maximizing the attenuation of the surrounding medium. In seawater, the attenuation rises significantly at the infrared and ultraviolet edges of the visible spectrum. The total attenuation constant c of clean seawater is approximately 0.4 m^{-1} at 670 nm and increases to 2 m^{-1} at 800 nm. Semiconductor lasers are readily available in this wavelength range and may be selected for a particular requirement of standoff distance.
Interference from solar radiation may be reduced further by selecting a wavelength corresponding to water or other absorption lines in the solar spectrum. The downwelling irradiance in water is severely curtailed at wavelengths in excess of 600 nm: At 5

meter depth the irradiance is about 10 nW cm^{-2} nm^{-1} in clear water, while at 25 m depth it is 0.03 nW cm^{-2} nm^{-1}. These figures are significantly smaller in the 670 nm to 800 nm wavelength range. Thus, the use of wavelength filtering methods in conjunction with typical interference filters (FWHM = 10 nm) can limit solar interference effects to a tolerable level in comparison to the detector noise equivalent power, without resorting to temporal modulation methods, if the operating depth is sufficiently large. To date, two prototype systems have been built using a 670 nm wavelength laser diode and operation is possible at greater than a 10-20 meter immersion depth in daylight conditions.

Tests of the configuration shown in Fig. 4 have been successful using a 10-milliwatt 670 nm semiconductor laser. Two instruments having different maximum standoff capabilities have been designed and constructed. Since the noise floor of the detector is approximately 10 nW_{pk}, the detected power of 6 μW_{pk} , provides a S/N ratio of 600:1, allowing substantially greater range resolution than the 200:1 initially considered. Imaging systems constructed to date have used steady-state optical excitation, with scan rates per pixel of 800 kHz.

4. DESIGN IN PROGRESS

A laser-based range mapping system is currently being developed by the authors under NSF and Duke University sponsorship. It will afford a method of collecting geological data not easily available by other means. Many of the techniques developed for land geology are usable on the seafloor; for example, making geological maps of seafloor exposures along a mid-ocean spreading region. A fundamental aspect of making geological maps is documentation of the orientation of various planes and lines in space. Geological terms, such as *strike* and *dip,* typically characterize planes, while *trend* and *plunge* characterize lines. Sedimentary bedding, lava flow tops, dike margins, igneous layering, metamorphic foliations, joints and faults are just a few examples of planar structures observed along spreading centers. Land geologists determine the orientation of outcrop-scale features with various types of hand-held compasses and inclinometers, like the Brunton Compass used widely in North America. However, this type of instrument is not suitable for use on the seafloor and a laser based method is preferred for underwater use. The laser approach allows surfaces of interest to be rapidly scanned producing high-resolution digital maps. The 3-D map coordinates combined with the measured roll and pitch angles of the instrument are used to accurately determine orientation of the scanned geologically relevant planes and lines on seafloor outcrops. Unlike other techniques currently in use, the optical scanner does not need to be carefully positioned or placed on the rock surface and is not affected by magnetic fields. Furthermore, due to the high scan rate, the instrument need not be stationary while scanning. The 3-D laser mapping system is expected to be used in studies of slope morphology, sedimentology, hydrothermal vents, biology, structural geology, and rock magnetism. Initial deployment is expected on Woods Hole's *Alvin* submersible next year.

The design requirement is similar to previous ones, but will operate at standoff distances to 3 meters. Because of the low reflectivity of the seafloor (<10%), and because of the depth along the mid-Pacific spreading regions, an 80 mW Nd:YAG laser was selected for the design. The configuration of the scanner was developed using Solid Works'98 3-D solid modeling software and the optical design package Trace-Pro. The prototype scan assembly is shown in Fig. 7.

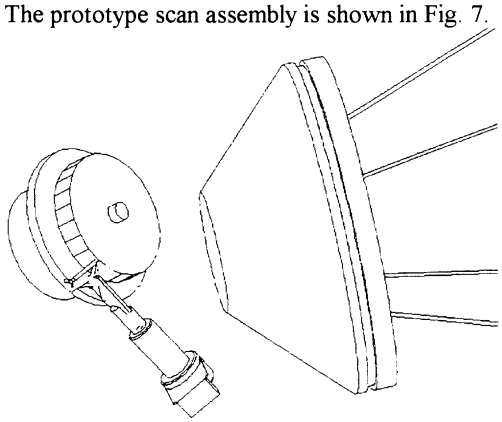

Fig. 7. Scanner design used in the prototype geological profiling system, showing optical pressure port (rightmost), rotating horizontal scan mirror (upper) and vertical scan galvanometer (lower). Laser scan limits are shown exiting the window.

A 24-facet rotating polygonal mirror is used to develop a horizontal line scan and a high-speed galvanometer is used for vertical deflection. The desired scan angles are limited by the window design for immersion to 20,000 feet. The maximum scan half-

A 24-facet rotating polygonal mirror is used to develop a horizontal line scan and a high-speed galvanometer is used for vertical deflection. The desired scan angles are limited by the window design for immersion to 20,000 feet. The maximum scan half-angle is 360/24 = 15 degrees. The immersion effect reduces the effective scan angle to +/- 15 x $(1.34)^{-1}$ = 11.2 degrees. The placement of the laser beam with respect to the polygon mirror and the y-axis tilt mirror is determined by the desired scan angle and mechanical considerations, such as component interference and window aperture. The component placement was restrained to prevent contact between the mirrors over their entire angular scan ranges and to minimize the window aperture. Two layouts were developed, one for a scan offset angle (θ at scan center in Fig. 2) of 40 degrees and one for a scan angle of 60 degrees. The scan limits were modeled and the minimum window aperture determined. The high external pressure requires the use of an acrylic window (pressure port) and design is based on work by Stachiw[26].

5. INTERFEROMETRIC IMAGING

Interferometric techniques can offer improvements in range resolution beyond that attainable from structured illumination methods and can potentially distinguish the light field returning from the scene from that generated by scattering or other effects. Although optical interferometric schemes (holography and correlation methods) have been investigated for use undersea, they rely upon the coherence of the illuminating source and intervening medium. A substantial amount of effort has been expended in this regard but system complexity and other factors have limited commercialization. An alternative to using coherency of the optical beam is to construct spatial or temporal gratings by modulation methods. One such system, suggested years ago for long range visibility improvement by one of the authors, has been recently demonstrated by Sandia National Laboratory under Navy sponsorship and is producing good range images in turbid water and through the air-water interface.

Another technique using spatially modulated projections, i.e. video moiré, relies upon interference of two spatial gratings and offers an alternative solution for resolving detail in the object contour. The scheme also is capable of enhanced imaging through turbid media using a spatial correlation detection method. In a collaborative effort between Florida Institute of Technology and Harbor Branch Oceanographic Institution, a moiré contouring system was demonstrated that generates real-time surface contours with zoom magnification capability. The system is particularly suited to underwater use since only one standard video camera is used in conjunction with a laser grating projector[2]. The potential for using real-time video moiré techniques to distinguish between damaged and undamaged areas on structures appears to be promising for underwater inspection applications but has yet to be proven in the field in real world conditions. In the classical projection moiré system, the distorted target grating is viewed through a physical reference grating. This reference grating has the effect of a binary optical filter in that opaque areas of the grating allow no information to be transmitted, while clear areas of the grating allow information to be passed. By using a special video processor this situation may be duplicated electronically. The output of the video processor circuit is an image showing equal depth moiré contours superimposed on the target.

6. SUMMARY

In this paper, we have reviewed techniques used for enhanced undersea image formation and have described recent developments in the formation of range map images. Although many systems are being developed using different ranging techniques, we have described a scanning laser triangulation method that relies upon a lateral effect photo-diode and micro-channel plate intensifier for detection. The 3-D surface mapping system has been demonstrated in short range (~1m) applications where real time (20 scan/s) analysis of objects in motion is necessary. The system is also configurable for longer distance image formation using higher power laser sources and/or slower scan rates. Another system suited for geological application is being developed presently for deployment along the mid-pacific rift and will be able to measure lava flow shape and orientation at a range of 2 to 3 meters. New systems will certainly utilize continuing advances in the efficiency, power output, and size of blue-green lasers, and will take advantage of advances in narrow-band, wide-aperture filter technology to reduce interference from ambient lighting.

7. ACKNOWLEDGMENTS

The support of the U. S. Navy under contract N47408-91-C-1209 is gratefully acknowledged for initial prototype development, as well as the National Science Foundation under grants OCE-9318399 and OCE-9814147 for advanced development. Additional support of the Atlantic Foundation for initial and supplemental system development is gratefully acknowledged, as well as the support of Dr. Jeffrey Karson at Duke University, who recognized the geological application of the technology.

8. REFERENCES

1. Caimi, F., and R. F. Tusting, "Application of Lasers to Ocean Research and Image Recording Systems," Proc. Intl. Conf. Lasers-87, pp. 518-524, 1987.

2. Caimi, F., J. Blatt, B. Grossman, et al., "Advanced Underwater Laser Systems for Ranging, Size Estimation, and Profiling," Marine Technology Society Journal, v. 27, No. 1, pp. 31-41, 1993.

3. Jaffe, J. and P. M. Casscreau, "Multimode Imaging for Underwater Robots," Proc. SPIE v. 768, pp. 107-111, 1987

4. Preisendorfer, R. W., Hydrologic Optics, vols. 1-6 Reports to the National Oceanic and Atmospheric Administration, NTIS PB-259 793, 1976.

5. Jerlov, N. G., *Marine Optics,* Elsevier Oceanography Series, Amsterdam, 1976.

6. Duntley, S. Q., "Light In The Sea", J. Opt. Soc. Am., 53, pp. 214-233, 1963.

7. Morel, A., "Optical Properties of Pure Water and Seawater," in *Opt Aspects Of Oceanography*, (N. Jerlov and E. S. Nielsen, eds. pp. 1-24, Academis Press, New York, 1974.

8. Hodara, H., "Refractive Index Variations in Seawater," AGARD Lecture Series 61 on Optics in the Sea, pp. 2.2-1-2.2-12, Neuilly Sur Seine, France, 1973.

9. Wells, W. H., "Loss of Resolution in Water as a Result of Multiple Small Angle Scattering in Water," J. Opt. Soc. Am., 59, 6, June 1969.

10. Wells, W. H., "Indirect Illumination to Reduce Veiling Luminance in Seawater," Proc. SPIE v. 1557, pp. 2-9, San Diego, July 1991.

11. Mertens, L. W., *In-Water Photography, Theory and Practice,* Wiley, New York, 1970.

12. Funk, C. J. , S. B. Bryant, and P. J. Heckman, " Handbook of Underwater Imaging System Design," Naval Undersea Center Report TP-303, July, 1972..

13. Jaffe J. and C. Dunn, "A Model Based Comparison of Underwater Imaging Systems," Proc. SPIE v. 925, Ocean Optics IX, pp. 344-350, 1988.

14. Karp, S., R. M. Gagliardi, S. E. Moran, and L. B. Stotts, *Optical Channels*, Plenum Press, New York, 1988.

15. Klepsvik, J. O., et al., "A Novel Laser Radar System for Subsea Inspection and Mapping," Proc. IEEE Oceans'94, Vol. II, pp. 700-705, Brest, Sept. 1994.

16. Swartz, B., "Laser Range Gate Underwater Imaging Advances," Proc. IEEE Oceans'94, Vol II, pp. 722-727, Brest, Sept. 1994.

17. Leatham, J. and B. W. Coles, "Use of Laser Sensors for Search and Survey," Proc. Intervention-93, pp. 171-186, 1993.

18. Strand, M., Personal communication, 1994.

19. Yu, Chi-Ho, and F. Caimi, "Determination of Horizontal Motion through Optical flow Calculations," Proc. IEEE Oceans'93, v. II, pp.475-480, Victoria, October 1993.

20. Negahandaripour, S., C.H. Yu, and A. Skokrollahi, "Recovering Shape and Motion from Underwater Images," IEEE J. Oceanic Engineering, V. 15, No. 3, pp. 189-198, 1990.

21. Klepsvik, J. O., and H. O. Torsen, " Recent Advances in Accurate Underwater Mapping and Inspection Techniques," Proc. International Ocean Technology Congress, Honolulu, January, 1989.

22. Caimi, F., and D. Smith, " Three Dimensional Mapping Systems and Methods," U.S. Patent 5,418,608, 1995.

23. Massey, J. "Underwater Laser Mapping for Ship Husbandry," Proc. Underwater Intervention-94, pp. 312-318, 1994.

24. Caimi, F. and A. Bessios, "Surface Mapping and Imaging Using Low-Power Lasers," Proc. IEEE Oceans'94, v. II, pp. 716-721, Brest, September, 1994.

25. Caimi, F., " AMNSYS Test Results, Unpublished Report, HBOI, 1992.

26. Moore, K., Jaffe, J., and Ocoha, L., "Development of a New Underwater Bathymetric Imaging System , J. OAOT, in review, 1999.

27. Stachiw, J. D., Acrylic Plastic Viewports, Marcel Dekker, NY, NY, 1982.

28. Scott, M. W., Range Imaging Laser Radar, US Patent# 4.935,616, Sandia National Laborarory.